Lamellar-Grating-Based MEMS Fourier Transform Spectrometer

Huseyin R. Seren, *Student Member, IEEE*, Sven Holmstrom, N. Pelin Ayerden, Jaibir Sharma, and Hakan Urey, *Senior Member, IEEE*

***Abstract*—Design, fabrication, and characterization of a high-performance micromachined lamellar-grating-interferometer-based Fourier transform spectrometer are presented. The device is designed to give high deflections with very low dynamic deformation and good mode separation. Mechanical self-stoppers are introduced to withstand accelerations larger than 500 g due to shock. The clear aperture area of the grating is about 10 mm^2. The maximum deflection while electrostatically actuated at ambient conditions is ± 356 μm at 71.2 V and 340 Hz, setting a record for comparable devices. At a pressure of 8.6 Pa, the same deflection is reached at 4.3 V. Six hundred eighty spectra per second can be recorded with a resolution of 14 cm^{-1}. With a HeNe laser at 633 nm, a spectral resolution of 0.54 nm (22 cm^{-1}) is reached using electrostatic actuation. The microelectromechanical systems device is integrated into a compact Fourier transform spectrometer setup including a blackbody source, an infrared (IR) detector, and a visible laser using the device back side for reference. Early results with IR interferograms are also reported. In addition, the devices are actuated with pressure waves in the ambient air to reach deflections up to ± 700 μm. With this setup, the spectrum of a red laser is measured with a resolution of 0.3 nm (12.4 cm^{-1}). [2011-0252]**

***Index Terms*—Fourier transform spectroscopy (FTS), infrared (IR) spectroscopy, interferometer, lamellar grating, microopto-electromechanical systems.**

I. Introduction

FOURIER transform spectroscopy (FTS) has evolved into a standard analytical technique in the fields of physical, biological, and chemical sciences, as well as a tool for quality and process control, bomb detection, mining industry, and gas detection. Compared to other spectroscopy methods, it provides high accuracy, high throughput, a compact form factor, and low cost. The conventional FTS devices make use of a Michelson interferometer configuration with a movable mirror in addition to a beam splitter and a stationary reference mirror. Due to machining limitations, dispersive techniques dominated spectrometry until the 1970s, when FTS started to take over. In 1960, Strong and Vanasse demonstrated the lamellar grating interferometer (LGI), which utilizes a dynamic binary diffraction grating with a variable depth and operates in the zeroth order of the diffraction pattern [1], [2]. With the improvements in microfabrication and microelectromechanical systems (MEMS) over the last two decades, these devices have become increasingly feasible to realize also for shorter wavelengths [3]. With the LGI configuration, several advantages follow. While the Michelson interferometers make use of a beam splitter to split wave amplitudes, in an LGI device, half of the wavefront is reflected from the moving grating mirror fingers, and the other half is reflected from the static grating mirror fingers, as shown in the system overview in Fig. 1. The displacement of the moving grating fingers determines the optical path difference (OPD). In effect, the LGI eliminates the need for the reference mirror, the beam splitter, and the dispersion compensation plates. This makes it possible to design high-performing spectrometers, which are more compact and robust than what is currently available. In addition, the assembly is simpler and less sensitive to vibrations than the Michelson setup.

The intensity of the zeroth order from the diffraction pattern of a laser beam reflected from the LGI is determined only by the

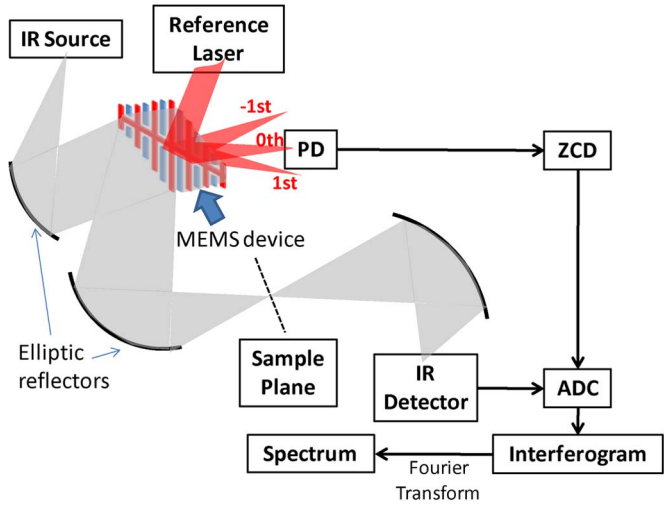

Fig. 1. Layout of the LGI-type FTS measurement system. The IR source is a blackbody source. The reference laser provides position feedback and the sampling clock. PD is a photodetector, ZCD is a zero-crossing detector, and ADC is an analog-to-digital converter.

Manuscript received August 24, 2011; revised November 21, 2011; accepted November 26, 2011. Date of publication January 18, 2012; date of current version April 4, 2012. This work was supported by the MEMFIS Project, supported by the European Commission Seventh Framework Program under Grant 224151. Subject Editor O. Solgaard.

H. R. Seren was with Koç University, Istanbul 34450, Turkey. He is now with the Laboratory for Microsystems Technology, Boston University, Boston, MA 02215 USA (e-mail: hrseren@gmail.com).

S. Holmstrom, N. P. Ayerden, and H. Urey are with the Optical Microsystems Laboratory, Department of Electrical and Electronics Engineering, Koç University, Istanbul 34450, Turkey (e-mail: sholmstrom@ku.edu.tr; nayerden@ku.edu.tr; hurey@ku.edu.tr).

J. Sharma was with Koç University, Istanbul 34450, Turkey. He is now with the Sensor and Actuator Microsystems Program, Institute of Microelectronics, Agency for Science, Technology and Research, Singapore 117685 (e-mail: jaibirs@rediffmail.com).

Color versions of one or more of the figures in this paper are available online at http://ieeexplore.ieee.org.

Digital Object Identifier 10.1109/JMEMS.2011.2180362

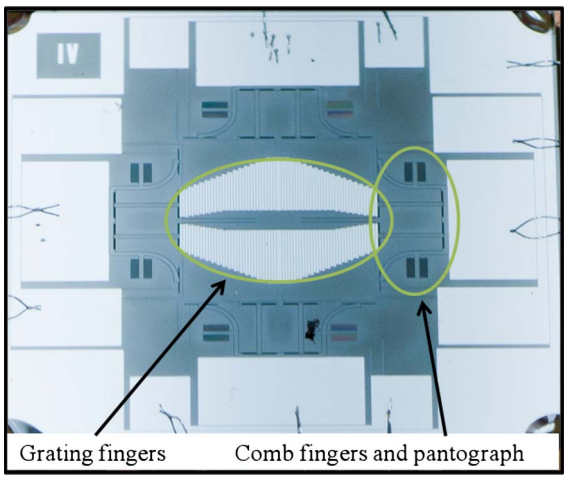

Fig. 2. Photograph of a wire-bonded MEMS device. The grating fingers, as well as one of the four sets of pantographs, are pointed out. Two comb-finger sets are connected to each pantograph.

spectral content of the illuminating light. If the change in OPD in the grating is known, the full spectrum of the light can be obtained through a Fourier transform of the zeroth-order interferogram. The optical considerations needed for the optimum performance of the LGI device have earlier been addressed by our group [4]. As stated there, the choice of grating period is necessarily a compromise between several factors to reach performance as high as possible for the desired wavelengths. On the one hand, the grating period has to be large enough to avoid Talbot reversal; on the other hand, larger grating period leads to increased mixing of the diffraction orders, reducing the signal-to-bias ratio (SBR).

The present study is carried out under the European Union Seventh Framework Program MEMFIS project, which aims to build an ultrasmall and portable midwave infrared (IR) spectrometer working in the 2.5-μm (4000 cm^{-1}) to 16-μm (625 cm^{-1}) range. This paper presents the design, fabrication, and characterization of an electrostatically actuated lamellar-grating-based spectrometer for the IR radiation using standard silicon-on-insulator (SOI) microfabrication. To this end, modified pantograph-type suspensions, originally introduced by the Fraunhofer Institute for Photonic Microsystems, are employed [5]–[7]. The main idea behind the pantograph spring is to create large out-of-plane motion through set levers connected with torsion springs. This is to avoid the bending mode, which requires soft levers. The device operates resonantly in the out-of-plane mode with the grating providing a large light collection mirror area compared to other microspectrometers reported in the literature [8], [9]. Primary challenges of the design are achieving large deflections without electrostatic pull-in of the structures, achieving $< \lambda/10$ flatness across a large clear aperture during dynamic deflections, and achieving resistance to large shock and vibrations for portable device applications. A wire-bonded MEMS device is shown in Fig. 2.

The optical, mechanical, and electrical designs are described in Section II. Device fabrication is described in Section III. The mechanical characterization is described in Section IV; interferogram acquisition and spectrum calculations are presented in Section V. In Section VI, this paper is concluded.

II. Microoptoelectromechanical Systems Design

A. Optical Design

For an LGI device, there are five major optical design considerations and limitations [4]. Two are shared with the conventional Michelson configuration: the total OPD in the interferometer and the IR source size. The latter is related to the beam divergence after the collimation optics. The third consideration is related to the size of the detector, which needs to be optimized to limit the mixing of zeroth- and first-order diffracted light from the grating. For this, there are a number of criteria that should be considered. First, the grating period should be selected so that the first diffraction order is separated enough from the zeroth order given the divergence of the light source and the distance to the photodetector. Otherwise, higher orders will reduce the interference at the zeroth-order signal and decrease the SBR. This is because a large dc signal would be added onto the information-carrying signal, and due to the dynamic range limitations of the photodetectors, this is not desired. This condition is given by (1) for a source half-divergence angle of $\alpha_{\text{divergence}}$, a wavelength of λ, and a grating period of Λ

$$\alpha_{\text{divergence}} \leq 0.5 \sin^{-1}\left(\frac{\lambda}{\Lambda}\right). \tag{1}$$

The fourth optical design consideration is the MEMS light efficiency, which is crucial for good signal-to-noise ratio and low power budget for battery-operated devices. To maximize the efficiency, the grating finger gap should be as small as possible, and the grating area should take up as much of the total illuminated area as possible. The gap was selected as 5 μm, since this is about the smallest gap which can be reliably achieved with our fabrication process. The shape of the backbone structure that holds the moving grating fingers is optimized with parametric finite-element modeling (FEM) simulations in a specialized software environment (ANSYS), so that the dynamic deformation on the backbone is kept within the limits for the smallest possible width. In addition, the beam shape should match the active device area as well as possible. Since a light source tends to generate a beam shape close to a circle, to avoid extra optical components, the active area should be designed in a more or less circular symmetric way. Lastly, the reflectivity of the grating coating should be maximized for the desired wavelength interval. Gold and aluminum both have good reflectivity in the mid-IR region. In this case, aluminum was chosen due to its larger compatibility with standard microfabrication processes.

The fifth optical consideration is again related to diffraction. If the grating period is kept too small with respect to the wavelength, light passing through the first set of grating fingers diverges too fast. Moreover, at the specific distances between the first and second sets of fingers, light can form the phase-reversed Talbot images, and most of the energy may then escape through the holes of the second set of grating fingers. This phenomenon degrades the acquired interferogram and, thus, the spectral resolution of the measurement when the path difference between grating finger sets becomes closer to the critical length.

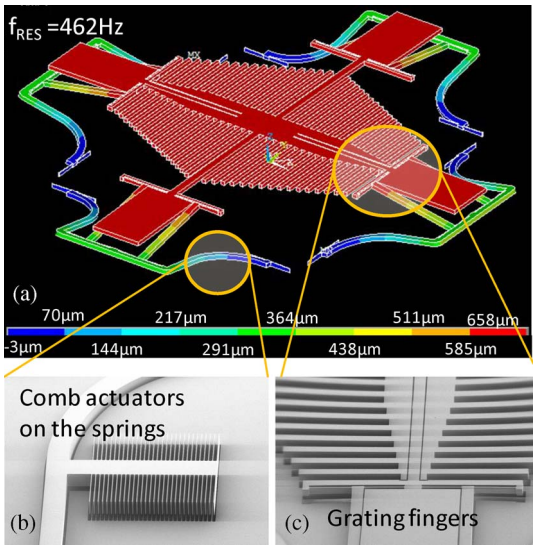

Fig. 3. (a) ANSYS FEM result of the first mode of the MEMS device at 462 Hz. The comb actuators along the spring are not modeled and are therefore not shown in this figure. For their relative placement, see Fig. 2. (b) SE micrograph of one set of comb fingers. The grating structure is predeflected out of plane by about 75 μm for this picture. (c) SE micrograph of a section of the grating fingers from the same device.

Talbot images appear at integer multiples of Z_{Talbot}, which is determined by

$$Z_{\text{Talbot}} = \frac{2\Lambda^2}{\lambda}. \tag{2}$$

The phase-reversed Talbot images appear in between the Talbot images, with the first one at $Z_{\text{Talbot}}/2$, effectively setting a deflection limit for the spectrometer to be useful in the measurement range of interest.

One of the most important design decisions is the choice of the grating pitch. Limits for the ideal case are set in opposite directions by (1) and (2). For a wavelength interval of 2.5–16 μm, $\alpha_{\text{divergence}} = 2.5°$, and a maximum deflection of 500 μm, the limits set on the grating pitch become $\Lambda < 28$ μm using the minimum wavelength (1) and $\Lambda > 90$ μm using the maximum wavelength (2). Since these limitations are conflicting, the final choice has to be done through compromise. The optical grating pitch was selected based on a detailed numerical analysis using two performance metrics: spectral resolution across the spectral band and SBR at the detector. In the light of the analysis in [4], we chose $\Lambda = 130$ μm grating period for the mid-IR band, limited by the detector used in our system. The clear aperture area of the grating is 10 mm^2.

B. Mechanical Design

The largest challenges for a MEMS spectrometer design are to be found in the mechanical requirements, since a very large stroke is needed while, at the same time, the active grating area has to remain flat during the resonant motion. The FEM model of the out-of-plane vibration mode of the device and two scanning electron (SE) micrographs of different sections can be seen in Fig. 3. The images were taken while the movable grating fingers were mechanically predeflected.

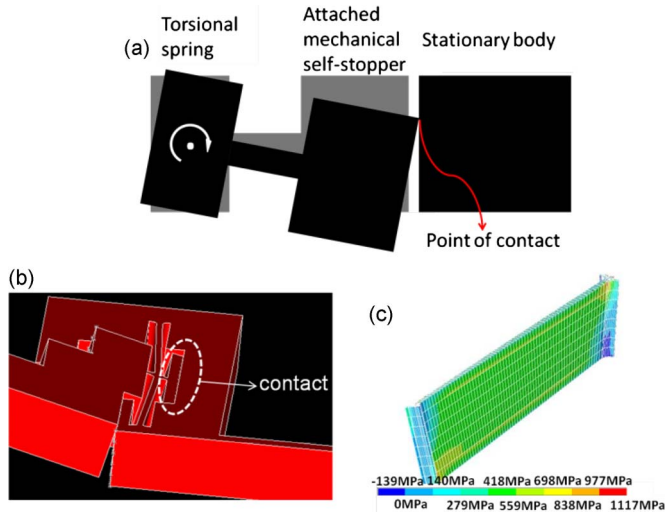

Fig. 4. (a) Sketch of the mechanical self-stoppers connected to the torsional springs, limiting the motion to about 700-μm deflection p–p (corresponding to 500-g acceleration). (b) Detail from the ANSYS FEM model illustrating the mechanical self-stoppers. (c) Stress distribution along one of the torsional springs from the FEM model. The maximum stress is ~1.1 GPa at 500 μm of one-sided deflection.

TABLE I
RESONANCE MODES BASED ON FEM ANALYSIS

Mode Number	Resonance Freq (Hz)	Mode Shape
1	462	Out-of-Plane
2	1160	Rocking
3	1183	Rocking
4	1422	Pantograph Out-of-Plane
5	1659	In-Plane
6	1660	In-Plane

Pantograph suspensions can create high out-of-plane strokes in a small area through a torsional motion conversion mechanism [Fig. 4(a)], which also efficiently confines the deformation to the spring. FEM software was used to model the mechanical structure. The springs are designed with regard to maximum stress levels to allow 500-μm out-of-plane deflection of the grating body without risk of breaking. Dual springs are used at each connection point to increase the operation survivability at large strokes (i.e., together they can supply the desired stiffness while performing large torsional rotations without reaching the stress limit). The largest expected stress on the springs according to the simulation is 1.1 GPa [Fig. 4(b)]. Another major goal in the mechanical design process is the mode placement. The desired out-of-plane mode should be the first mode, and all higher resonance modes need to be far enough above the first mode to avoid mode coupling. Close modes can cause parasitic distortions and affect the device performance. Therefore, the spring dimensions are picked so that the second mode is at a frequency between the second and third harmonics of the first mode (Table I).

For a portable field device, the MEMS die needs to be robust and survive large impacts. To serve this purpose, mechanical stops were designed to limit the out-of-plane motion and to protect the springs from excessive stress. After passing the

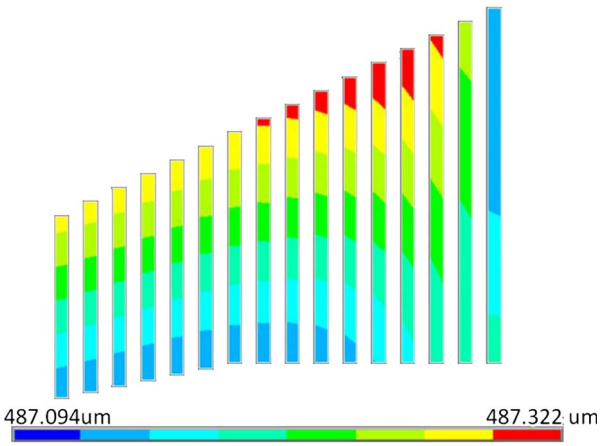

Fig. 5. FEM of dynamic deformation distribution of the grating fingers in one quadrant in ANSYS. The scale shows the out-of-plane displacement amplitude. The deformation is 226 nm p–p, less than $\lambda/10$, for $\lambda_{\min} = 2.5$ μm at 487-μm zero-to-peak deflection. The dynamic deformation scales linearly with deflection.

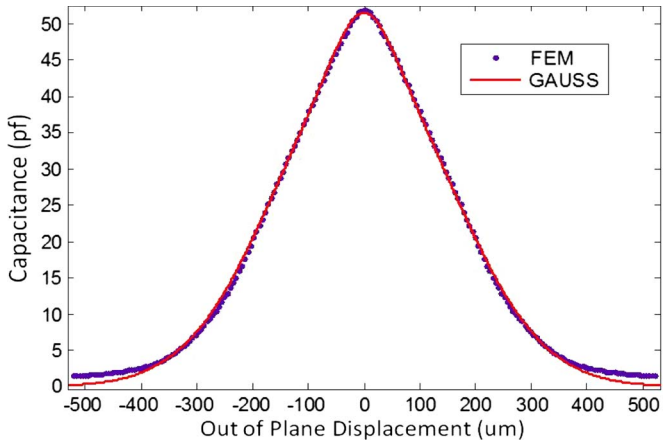

Fig. 6. Simulated capacitance change with Gauss fit. The graph assumes that comb fingers, as well as the grating fingers, are used for actuation, effectively doubling the capacitance compared to how the devices were actually actuated.

deflection limit, mechanical stop structures come to a contact as a result of rotation and translation of the pantograph arms [Fig. 4(c)]. This increases the effective stiffness by providing resistance against accelerations as large as 500 g. For the devices with mechanical stoppers, the motion will be brought to a halt at a deflection of about 500 μm in either direction.

Dynamic deformation is yet another critical issue for resonant devices. Much effort was spent to minimize the dynamic deformation. For the optimized structure, peak-to-peak (p–p) deformation on the grating fingers is around 230 nm for 500-μm deflection, which is an acceptable design point (Fig. 5). Dynamic deformation scales linearly with the deflection and scales quadratically with the resonance frequency [10], [11]. Therefore, we reduced the resonant frequency in order to reduce the dynamic deformation to acceptable levels. The thickness of the device is 75 μm, which was sufficient to keep the deformation within the limits of the design goal. However, the most crucial advancement made toward reducing the deformation was adding decoupling suspensions at the joints of the pantographs. When the pantographs are directly connected to the body, the middle portion of the structure tends to bow, and deformations on the order of a couple of micrometers are thus created. These long and flexible suspensions on all four sides transfer the motion directly to the center of the grating structure and absorb most of the deformation themselves. The joint positions of these suspensions and the length of the grating fingers are optimized by parameter sweeping in ANSYS.

C. Electrical Design

It has been shown in several earlier publications that there is no need for an intentional vertical offset for resonant actuation of MEMS actuators [6], [12]–[14]. Unavoidable fabrication aberrations will always be sufficient to excite the resonant modes when excited properly. The dependence of actuation torque on the displacement creates time-varying torsional stiffness, resulting in a typical parametric-type system [13], [15], [16]. For parametric oscillators, the expression $2f_r/n$, where f_r is the mechanical resonance frequency and n is a positive integer, describes the placement of the subharmonic oscillations. The amplitude of the oscillation decreases with higher values of n. Given the parametric nature of the device, the maximum deflection will obviously be found when actuated at twice the mechanical resonance frequency of the mode in question. Physically, this means that the voltage has to be turned on twice per cycle of motion. To impart force from the actuation signal, eight sets of comb fingers are placed along the sides of the pantographs. These comb sets are composed of 200-μm-long, 5-μm-wide, and 75-μm-deep fingers, creating a capacitance of around 26 pF (Fig. 6). The change in capacitance as a function of out-of-plane displacement in Fig. 6 was simulated with the ANSYS CMATRIX macro. This information was used to calculate the required voltage level by numerically solving the equation of motion. During the modeling of the devices, it was assumed that, in addition to the comb fingers, the drive signal would simultaneously be connected to the grating fingers. The grating fingers would supply 25 pF, doubling the total capacitance.

Finger pull-in is a common problem for electrostatic comb-drive devices. This was simulated through worst case scenario models for our grating and comb-drive fingers by using the complete asymmetric case. The pull-in voltage for the longest grating finger is theoretically found as 95 V, whereas it is 160 V for comb-drive set fingers. During characterization, it was discovered that using the grating fingers for the actuation created instability, causing pull-in. This happened much earlier than predicted by the finger pull-in calculation above. Because of this, all tests were carried out by only using the comb fingers for actuation while electrically shorting the fixed grating fingers with the moving parts. As will be discussed further in the section on mechanical characterization, these types of systems show hysteretic behavior. This kind of behavior is widely examined in [12], [17], and [18]. According to the modeling results, the expected result was to reach a 1000-μm p–p stroke using a square-wave excitation of 50 V with a dc offset of 25 V.

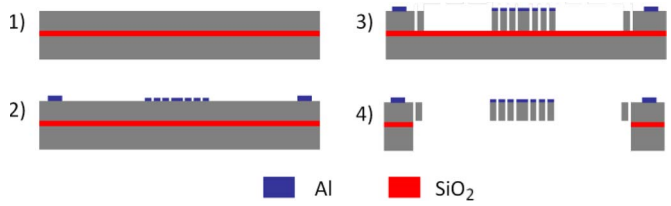

Fig. 7. Fabrication scheme is a standard four-mask SOI process. The first two masks are used for metallization. Masks 3 and 4 are used to define the front- and back-side DRIE, respectively.

III. Fabrication of LGI Devices

The devices are fabricated with a standard four-mask SOI process, using two masks for silicon deep reactive-ion etch (DRIE) and two masks for metal patterning. The SOI wafers have a 350-μm-thick handle layer, a 1- or 2-μm-thick buried oxide (BOX), and a 75-μm device layer [Fig. 7(1)]. The thickness of the latter determines the thickness of the entire mechanical structure. At the start of the process, 400 nm of Al is blanket sputtered onto the device side of the wafer. Photolithography using mask 1 is followed by metal etch to form metal pads, needed for electrical connections. A much thinner layer of 60-nm Al is then blanket deposited onto the wafer and patterned with mask 2 to define the interferometer grating. For both steps of metal patterning, 2 μm of AZ1512 resist is used [Fig. 7(2)]. The entirety of the mechanical parts of the device is defined by mask 3, followed by front-side DRIE, using the BOX as etch stop [Fig. 7(3)]. Through back-side lithography with mask 4 and a final DRIE step, back-side windowing and device dicing are realized. For the front- and back-side silicon etch, 5 and 10 μm of AZ9260 resist, respectively, are used as etch masks. The final device release is achieved with oxide etch in HF vapor [Fig. 7(4)].

IV. Mechanical Characterization

The resonant behavior of the devices was characterized with the help of a laser Doppler vibrometer (specifically Polytec products OFV-2500 and OFC-534). Before any characterization, the devices are glued and wire bonded to one of two different types of specially designed printed circuit board mounts. The expected resonance frequency according to the FEM simulations was 462 Hz. In practice, all devices turned out to have lower frequencies. The reason for the difference is unexpected thinning of the flexures during the front-side DRIE fabrication step. Optical microscopy measurements established that the flexures were 1–1.5 μm thinner than designed. For all the devices used for Figs. 8 and 9, the out-of-plane resonance frequencies were found to be between 325 and 342 Hz at a voltage of 50 V p–p. When actuated with a voltage over the grating fingers, a structural pull-in occurred already at 25 V, much earlier than expected from the pull-in calculations. The observed pull-in was not due to weakness of single fingers but rather due to device instability. Because of this, all the data presented are taken with the moving part and the fixed grating fingers shorted to each other and with actuation force from the comb fingers only.

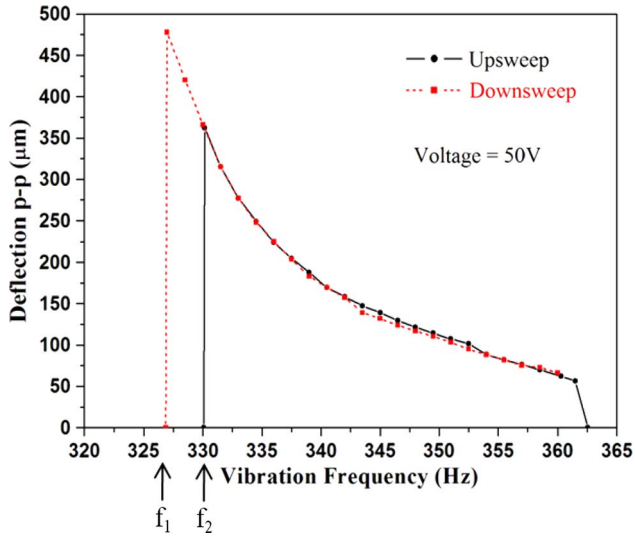

Fig. 8. Frequency response curves at 50 V, highlighting the hysteretic behavior due to electrostatic spring softening. f_1 and f_2 are the two jump frequencies close to the peak. Note that the mechanical vibration is taking place at half of the actuation frequency.

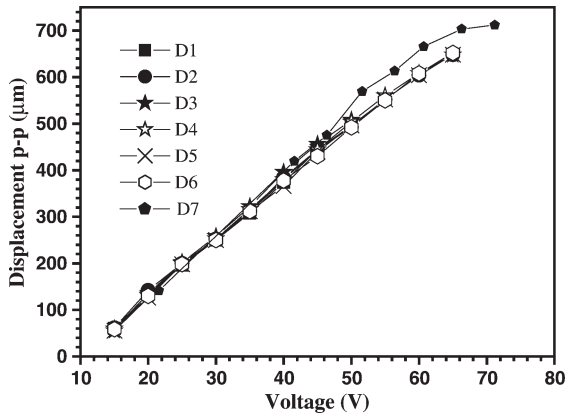

Fig. 9. Voltage response curves for several scanners. Scanner D7 was mounted on an alternative substrate, explaining the somewhat different characteristics of this device. The frequency is adjusted at each data point to match the resonance at that voltage level.

The device is actuated with a square wave with 50% duty cycle and an offset of half the p–p amplitude. Because of the parametric traits of the structure when electrostatically actuated, the maximum deflection will be achieved when the vibration frequency is equal to half of the excitation frequency. Fig. 8 shows the hysteretic frequency response of one device at ambient conditions. The curves exhibit the typical attributes for electrostatic spring softening [15], [19]. The spring softening behavior becomes more pronounced with increasing amplitude. At high amplitudes, there are two distinct jump frequencies f_1 and f_2. The first one jumps down from the maximum amplitude to zero during the downsweep, and the second brings the motion from zero up to the maximum amplitude of the upsweep. The voltage response curves of seven devices are shown in Fig. 9. For each data point, the frequency is adjusted to match the resonance at that voltage level.

To investigate the minimum voltage needed to get full deflection, the device was placed in a chamber with a pressure

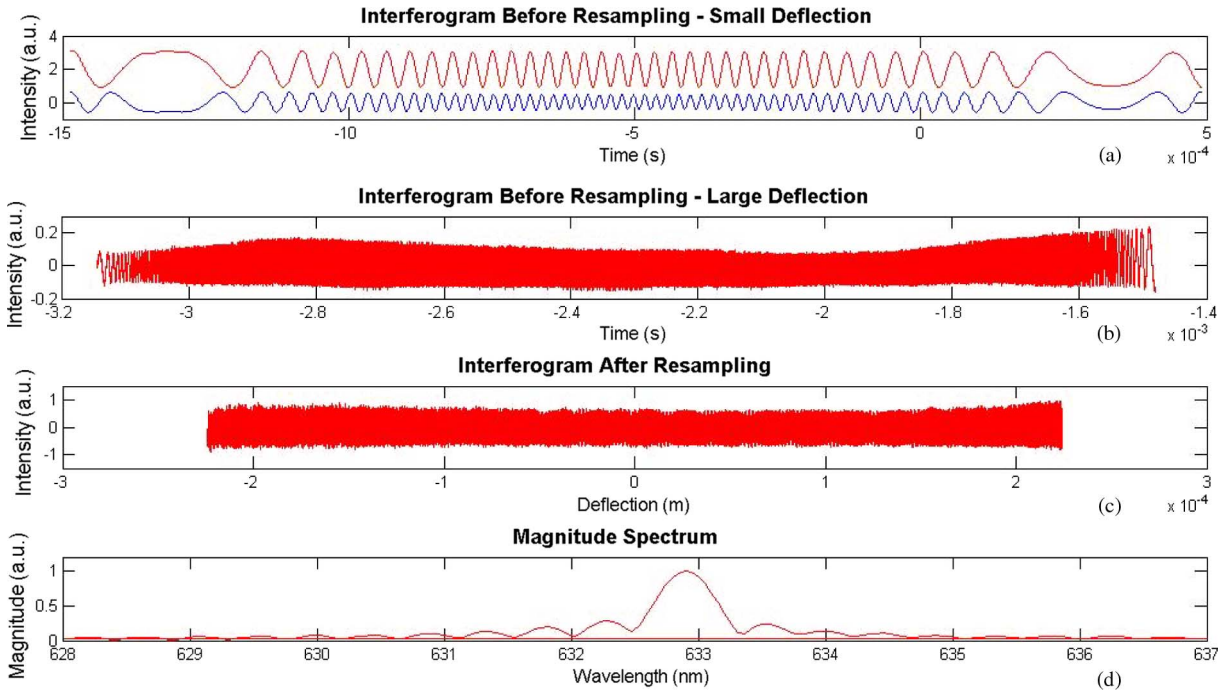

Fig. 10. (a) Interferograms are measured with a red 632.8-nm laser, together with a 408-nm blue reference laser. These data are taken at a very low deflection of 11 μm to make all details visible. (b) Interferogram before resampling for electrostatic actuation with 50 V at 296 Hz, giving a deflection of 448.4 μm p–p. The dc offset is subtracted from the interferogram. (c) Red laser after resampling. The x-axis indicates the physical deflection of the movable grating from the static grating. The OPD is at any given point double the absolute value of the deflection. (d) Fourier transformation of the signal in (c) results in a 0.54-nm FWHM peak at 15 802.78 cm^{-1}, corresponding to 632.8 nm.

reduced to 8.6 Pa. In this environment, a deflection of ± 350 μm was reached with a drive voltage as small as 4.3 V.

The strong spring softening behavior when actuated electrostatically makes it difficult to correctly measure the mechanical quality factor. To get around this problem, one device was instead actuated by vibrations in ambient air. By placing the device in front of a speaker vibrating at the resonance of the device, a full deflection could be attained using sound pressure. Actuated this way, as expected, the (electrostatic) spring softening effect and parametric behavior disappeared and were replaced by a smaller spring stiffening effect with nonzero amplitude on both sides of the jump discontinuities [20]. Since the parametric behavior stems from the electrostatic drive, a device driven by sound pressure will have its maximum response when actuated exactly at resonance. To measure the quality factor, a recently published formula for calculating quality factors from nonlinear frequency responses with jump discontinuities was used [21]. The mechanical quality factor was calculated to be 31. A different MEMS spectrometer design without the mechanical self-stoppers actuated this way gave a deflection of ± 700 μm.

V. Spectrum Measurements

If a resonating out-of-plane-mode comb structure is used as a diffraction grating, the intensity I_{center} recorded by a detector placed at the center of the diffraction plane as shown in Fig. 1 can be calculated as

$$d(t) = d_{\max} \cos(2\pi f_{\text{res}} t) \quad (3)$$

$$I_{\text{center}} = A \cos^2 (2\pi d(t)/\lambda) \quad (4)$$

where $d(t)$ is the vertical displacement of the grating and f_{res} is the resonance frequency of the comb structure [13]. Since the displacement of the device is sinusoidal [as expressed in (3)], the resulting intensity signal will be a chirped sinusoid. This chirp can easily be corrected by interpolation and resampling to produce a spatially equidistant interferogram which has a period of $\lambda/2$. To facilitate the resampling, a monochrome source with a known wavelength and a separate detector is typically used. A fast Fourier transform (FFT) operation performed on the resampled signal directly gives the spectrum of the illuminating light. All spectrum acquisition experiments described were performed in ambient conditions. The targeted stroke of ± 500 μm equals an OPD of 1 mm. Since the maximum theoretical resolution is given as $\Delta\nu = 1/OPD$, this would give an upper limit of 10 cm^{-1}. For full-width at half-maximum (FWHM), the expected value becomes $\Delta\nu = 0.6/OPD$ [22] or 6 cm^{-1} at 1-mm OPD. In this paper, spectral width measurements are reported as FWHM in nanometers, while the corresponding wavenumber estimations are reported using $1/OPD$. The present maximum OPD with electrostatic actuation of 0.712 mm yields a theoretical resolution of 14 cm^{-1}.

A first simplified setup was built with a red 632.8-nm (15 803 cm^{-1}) HeNe laser as the source and an ordinary photodiode placed at the zeroth order. A blue 408-nm laser diode illuminating the back side of the grating structure was used as reference [Fig. 10(a)]. After resampling the signal in MATLAB at the peaks and zero crossings of the interferogram of the reference laser, the wavelength of the red laser could be well determined with an FWHM of 0.54 nm (21.6 cm^{-1}) [Fig. 10(b)]. This should be compared to the theoretical

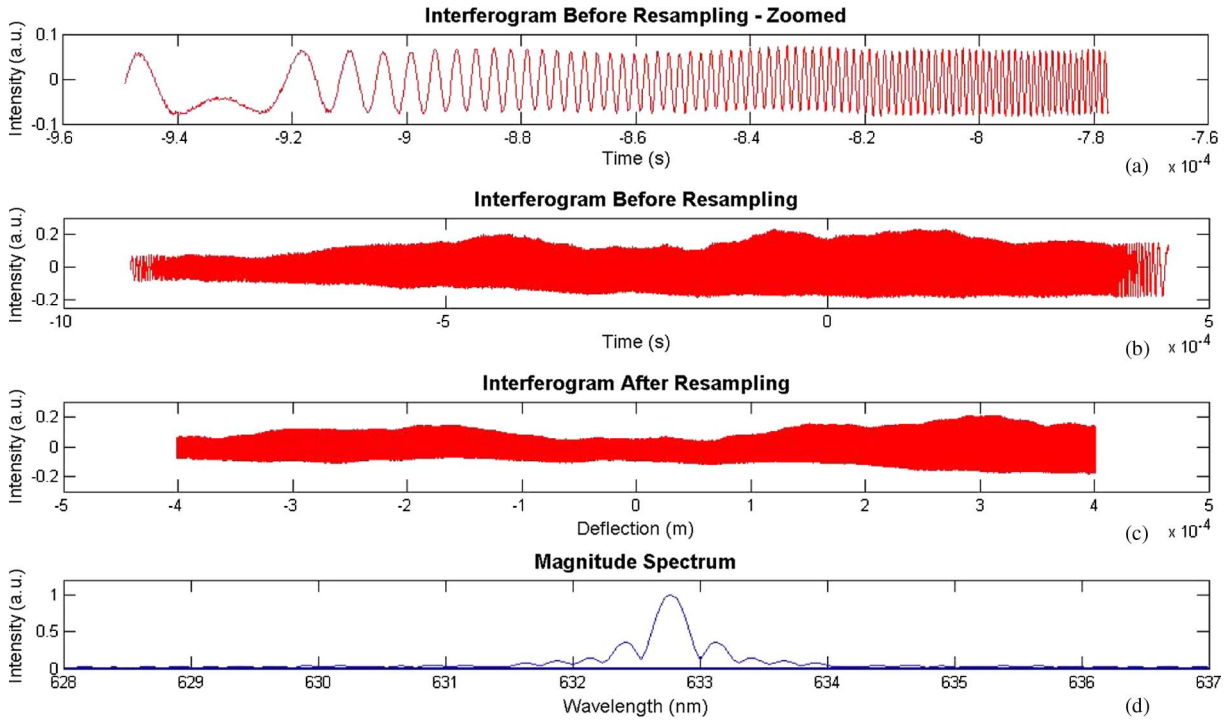

Fig. 11. (a) Zoomed view of the laser interferogram from a scanner without mechanical stoppers actuated by sound pressure. The deflection is 803 μm p–p at a resonance of 361.7 Hz. (b) Full interferogram used before resampling with its dc offset removed. (c) Interferogram after resampling in MATLAB to get equidistant sample points. (d) Resulting peak after transformation is 0.3 nm at FWHM, which is equal to the theoretical measurement resolution.

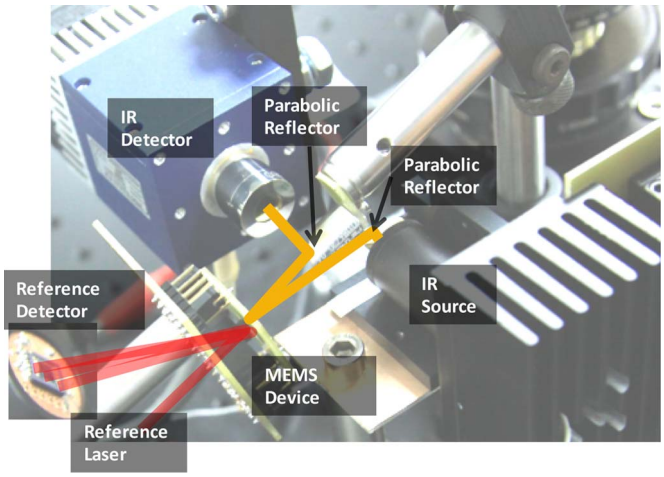

Fig. 12. FTS measurement setup used for the demonstrations.

resolution of 22.3 cm^{-1}, which is equal to an FWHM resolution of 0.54 nm and agrees very well with our measurements [Fig. 10(c)]. For this measurement, the device was operating at 296 Hz with a 50-V p–p input voltage, resulting in a deflection of 448.4 μm p–p.

The alternative design without mechanical stoppers, mentioned in the previous section, was actuated with sound pressure to create a spectrum while deflecting 803 μm p–p at 361.7 Hz (Fig. 11). The same red laser as above could now be resolved with an FWHM of 0.3 nm (12.4 cm^{-1}), which is equal to the theoretical value within the measurement resolution.

For IR measurements, the setup shown in Fig. 12 was assembled on an optical table. The IR source and detector are developed specifically for the MEMFIS project by Bruker Optics and Vigo System, respectively [23]. The detector is thermoelectrically cooled, continuously integrating, and of the mercury cadmium telluride type. The source is a blackbody radiator at 1070-K temperature with an emission diameter of only 0.5 mm. The beam is collimated by an off-axis parabolic mirror with 5.8-mm focal length. After the beam is reflected from the slightly inclined MEMS device, the second off-axis parabolic mirror with 20-mm focal length collects and focuses it onto the detector, where the interferogram is captured. There is no place for the sample in this arrangement, but it can be arranged by adding an additional optical relay. For optical feedback, a reference laser is sent at an off-axis angle to the back side of the device. The zeroth order is collected by the photodetector, as shown in Fig. 13(a). Both laser and IR interferograms are recorded by a data acquisition card. After filtering, the IR signal is sampled at the zero crossings of the reference in MATLAB to obtain spatially equidistant samples. The resulting IR interferogram can be found in Fig. 13(b). Next, Fourier transform is applied, and the spectrum of the source is obtained [Fig. 13(c)]. For the data in Fig. 13, the device was vibrating at 259 Hz with a deflection of 533 μm p–p. The quality of the IR and laser fringes in Figs. 10 and 13 shows that the static and dynamic flatness is at acceptable levels and the device does not have any significant mode-coupling problems. The resolution here is limited by the presently available data acquisition system. Higher resolution IR interferogram and spectrum computation requires a better data acquisition setup with higher dynamic range and further postprocessing. This, as well as expanding the setup to enable spectrum measurements of samples, is left as future work.

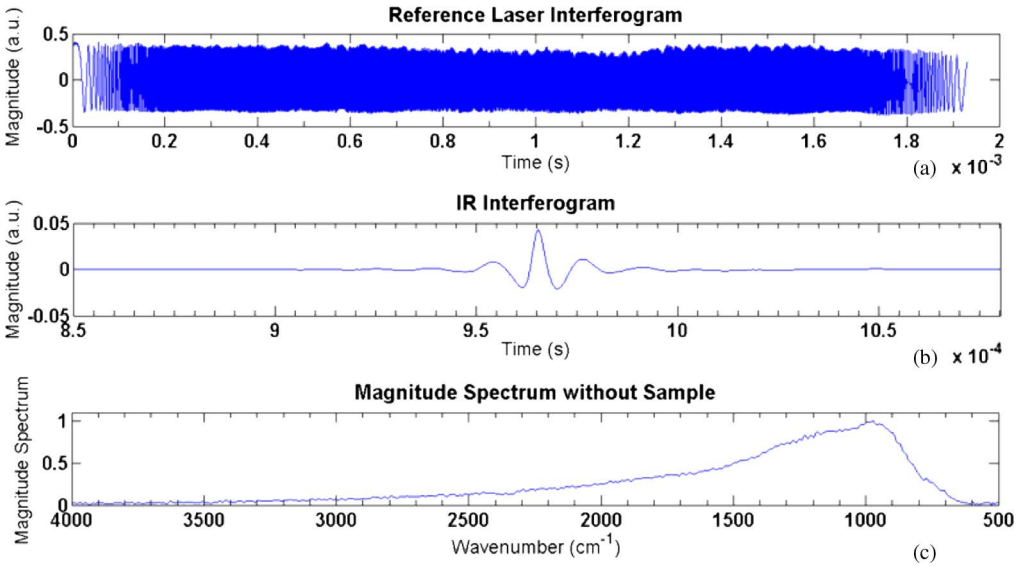

Fig. 13. (a) Reference laser interferogram. The data are taken at 50-V p–p input voltage at a resonance frequency of 259 Hz, resulting in 533-μm p–p deflection. (b) Simultaneous IR interferogram from a broadband source with 1070-K blackbody radiation. (c) Spectrum of the source obtained by applying FFT to the resampled IR interferogram.

VI. Conclusion

The characterization of the present MEMS stage, designed to be used as the active mechanical part of an LGI spectrometer, has shown that it has a large and stable stroke and can obtain IR and visible range interferograms. The obtained resolution at the visible range has been proven to meet the theoretical limit. The presented device can achieve an OPD of 712 μm and perform 680 scans/s. On the mechanical side, the device naturally has the advantage of long grating fingers which can be used as a comb-drive set. For the tests presented here, only the smaller comb fingers have been used, not the grating fingers. The capacitance provided by the grating fingers is 26 pF, which is almost equal to 25 pF from the comb fingers. Using the grating fingers not only as an optical component but also for additional actuation force would greatly lower the actuation voltage levels. This is certainly possible but requires some minor modifications to the design.

There are also two additional results pointing to further capabilities with a device of this type. First, the very low voltage requirement for operation at decreased pressure shows that it would be possible for a device like this one to be driven from a standard integrated circuit, without the need of high voltage, traditionally required by high-performing electrostatic devices. Second, a similar device without mechanical stoppers was shown to deflect 1.4 mm p–p while actuated by sound pressure; this is the highest performance achieved with such a large active area using MEMS technology. This shows the possibility of MEMS spectrometers with operating ranges far above our stated goal of 1-mm p–p deflection and that they can be driven at peak performance also in ambient without the use of the high voltages required by the electrostatic drive.

Acknowledgment

The authors would like to thank all MEMFIS partners, particularly T. Sandner from the Fraunhofer Institute for Photonic Microsystems, A. Piotrowski from Vigo System, A. Kenda from Carinthian Tech Research, and S. Lüttjohann from Bruker Optics for their contributions to the mechanical and optical designs. The microfabrication in this work was performed at the Center of Microtechnology (CMI), École Polytechnique Fédérale de Lausanne (EPFL), Lausanne, Switzerland, with the support of the CMI staff. The authors would also like to thank P. Flückiger and Y. Leblebici from EPFL, and E. Ermek, A. Mostafazadeh, and S. Ölçer for the help with the laboratory work.

References

[1] P. R. Griffiths, *Fourier Transform Infrared Spectrometry*. New York: Wiley, 1986.
[2] J. Strong and G. A. Vanasse, "Lamellar grating far-infrared interferometer," *J. Opt. Soc. Amer.*, vol. 50, no. 2, pp. 113–118, Feb. 1960.
[3] O. Manzardo, R. Michaely, F. Schädelin, W. Noell, T. Overstolz, N. De Rooij, and H. P. Herzig, "Miniature lamellar grating interferometer based on silicon technology," *Opt. Lett.*, vol. 29, no. 13, pp. 1437–1439, Jul. 2004.
[4] O. Ferhanolu, H. R. Seren, S. Lüttjohann, and H. Urey, "Lamellar grating optimization for miniaturized Fourier transform spectrometers," *Opt. Exp.*, vol. 17, no. 23, pp. 21289–21301, Nov. 2009, DOI: 10.1364/OE.17.021289.
[5] A. Tortschanoff, A. Kenda, M. Kraft, W. Scherf, T. Sandner, and H. Schenk, "Improved MOEMS based ultra rapid Fourier transform infrared spectrometer," *Proc. SPIE*, vol. 7319, p. 73190I, Apr. 2009, DOI: 10.1117/12.818646.
[6] T. Sandner, C. Drabe, H. Schenk, A. Kenda, and W. Scherf, "Translatory MEMS actuators for optical path length modulation in miniaturized Fourier-transform infrared spectrometers," *J. Micro/Nanolith. MEMS MOEMS*, vol. 7, no. 2, p. 021006, Jul. 2008, DOI: 10.1117/1.2945227.
[7] T. Sandner, A. Kenda, C. Drabe, H. Schenk, and W. Scherf, "Miniaturized FTIR-spectrometer based on optical MEMS translatory actuator," *Proc. SPIE*, vol. 6466, p. 646 602, 2007.
[8] O. Manzardo, H. P. Herzig, C. R. Marxer, and N. F. de Rooij, "Miniaturized time-scanning Fourier transform spectrometer based on silicon technology," *Opt. Lett.*, vol. 24, no. 23, pp. 1705–1707, Dec. 1999.
[9] W. Kenda, R. Scherf, H. Hauser, and H. Grüger, "A compact spectrometer based on a micromachined torsional mirror device," in *Proc. IEEE Sensors*, Vienna, Austria, May 2004, pp. 1312–1315.
[10] H. Urey, "Torsional MEMS scanner design for high-resolution display systems," *Proc. SPIE*, vol. 4773, pp. 27–37, Jul. 2002.

[11] P. J. Brosens, "Dynamic mirror distortions in optical scanning," *Appl. Opt.*, vol. 11, no. 12, pp. 2987–2989, Dec. 1972.
[12] C. Ataman and H. Urey, "Modeling and characterization of comb-actuated resonant microscanners," *J. Micromech. Microeng.*, vol. 16, no. 1, pp. 9–16, Jan. 2006.
[13] C. Ataman, H. Urey, and A. Wollter, "A Fourier transform spectrometer using resonant vertical comb actuators," *J. Micromech. Microeng.*, vol. 16, no. 12, pp. 2517–2523, Dec. 2006.
[14] H. Urey and A. Ataman, "Fourier transform spectrometer," E.P. Patent 1 677 086, Jul. 5, 2006.
[15] A. Arslan, D. Brown, W. O. Davis, S. Holmstrom, S. K. Gokce, and H. Urey, "Comb actuated resonant torsional microscanner with mechanical amplification," *J. Microelectromech. Syst.*, vol. 19, no. 4, pp. 936–943, Aug. 2010.
[16] K. L. Turner, S. A. Miller, P. G. Hartwell, N. C. MacDonald, S. H. Strogatz, and S. G. Adams, "Five parametric resonances in a microelectromechanical system," *Nature*, vol. 396, no. 6707, pp. 149–152, Nov. 1998.
[17] C. Ataman and H. Urey, "Nonlinear frequency response of comb drive microscanners," *Proc. SPIE*, vol. 5348, pp. 166–174, Jan. 2004.
[18] H. Schenk, P. Durr, T. Haase, D. Kunze, U. Sobe, H. Lakner, and H. Kuck, "Large deflection micromechanical scanning mirrors for linear scans and pattern generation," *IEEE J. Sel. Topics Quantum Electron.*, vol. 6, no. 5, pp. 715–722, Sep./Oct. 2000.
[19] S. K. De and N. R. Aluru, "Full-Lagrangian schemes for dynamic analysis of electrostatic MEMS," *J. Microelectromech. Syst.*, vol. 13, no. 5, pp. 737–758, Oct. 2004.
[20] A. M. Elshurafa, K. Khirallah, H. H. Tawfik, A. Emira, A. K. S. Abdel Aziz, and S. M. Sedky, "Nonlinear dynamics of spring softening and hardening in folded-MEMS comb drive resonators," *J. Microelectromech. Syst.*, vol. 20, no. 4, pp. 943–958, Aug. 2011.
[21] W. Davis, "Measuring quality factor from a nonlinear frequency response with jump discontinuities," *J. Microelectromech. Syst.*, vol. 20, no. 4, pp. 968–975, Aug. 2011.
[22] C. Ataman, "MEMS scanner for spectrometer and laser scanner systems," Ph.D. dissertation, Dept. Elect. Eng., Koç Univ., Istanbul, Turkey, 2008.
[23] A. Kenda, S. Lüttjohann, T. Sandner, M. Kraft, A. Tortschanoff, and A. Simon, "A compact and portable IR analyzer: Progress of a MOEMS FT-IR system for mid-IR sensing," *Proc. SPIE*, vol. 8032, p. 803200, Apr. 2011.

Huseyin R. Seren (S'10) received the B.S. and M.S. degrees in electrical engineering from Koç University, Istanbul, Turkey, in 2007 and 2009, respectively. He is currently working toward the Ph.D. degree in mechanical engineering in the Laboratory for Microsystems Technology, Boston University, Boston, MA.

His research interests include optical MEMS, RF MEMS, and functional metamaterials.

Mr. Seren was the recipient of The Scientific and Technological Research Council of Turkey (TÜBİTAK) Graduate Scholarship in 2007 and the Boston University Dean's Scholarship in 2009.

Sven Holmstrom received the M.Sc. degree in engineering biology from Linköping University, Linköping, Sweden, in 2005.

Since 2005, he has been a Research Engineer with the Optical Microsystems Laboratory, Department of Electrical and Electronics Engineering, Koç University, Istanbul, Turkey. During his time there, he has spent a sizable part of his time at Chalmers University of Technology, Gothenburg, Sweden, and the École Polytechnique Fédérale de Lausanne, Lausanne, Switzerland. His research interests include microfabrication and microoptoelectromechanical systems.

N. Pelin Ayerden received the B.Sc. degree majoring in electronics from Boğaziçi University, Istanbul, Turkey, in 2009. She is currently working toward the M.Sc. degree at Koç University, Istanbul, under the supervision of Prof. Hakan Urey working as both Research Assistant and Teaching Assistant.

She is working on the MEMFIS project that is aiming to design and fabricate an ultrasmall MEMS FTIR spectrometer. Her research interests include optical and biorelated MEMS applications.

Jaibir Sharma received the M.Sc. degree in physics from Chaudhary Charan Singh University, Meerut, India, in 1995, and the M.Tech. degree in solid-state technology and the Ph.D. degree in electrical engineering from the Indian Institute of Technology (IIT) Madras, Chennai, India, in 2000 and 2010, respectively.

He had good exposure to both industry and teaching before joining the Ph.D. program at IIT Madras in the year 2004. From March 2010 until the end of December 2010, he was a Postdoctoral Fellow at Koç University, Istanbul, Turkey. He is currently a Scientist with the Institute of Microelectronics, Agency for Science, Technology and Research, Singapore, working on module integration of MEMS with CMOS. His research interests are in MEMS reliability, cost-effective MEMS techniques, MEMS modeling, optical MEMS, optical-MEMS-based biosensors, metal–oxide–semiconductor device modeling, thin-film encapsulation for MEMS devices, and integration of MEMS with CMOS devices.

Hakan Urey (M'92–SM'09) received the B.S. degree in electrical engineering from Middle East Technical University, Ankara, Turkey, in 1992, and the M.S. and Ph.D. degrees in electrical engineering from the Georgia Institute of Technology, Atlanta, in 1996 and 1997, respectively.

After completing the Ph.D. degree, he joined Microvision, Inc., Seattle, WA, as a Research Engineer, and he played a key role in the development of scanning display technologies. He was the Principal System Engineer when he left Microvision, Inc., in 2001, to join the College of Engineering, Koç University, Istanbul, Turkey, where he established the Optical Microsystems Laboratory. He is currently a Professor of electrical engineering at Koç University. He has published more than 40 journal and more than 100 conference papers, six edited books, and four book chapters, and he has 21 issued and several pending patents. His research interests are in microelectromechanical systems, micro-optics, microoptoelectromechanical systems design, and laser-based 2-D/3-D display and imaging systems.

Dr. Urey is a member of SPIE, OSA, and the IEEE Photonics Society and the Vice-President of the Turkey Chapter of the IEEE Photonics Society. He was the recipient of the Werner von Siemens Faculty Excellence Award from Koç University in 2006, the Distinguished Young Scientist Award from the Turkish Academy of Sciences in 2007, and the Encouragement Award from The Scientific and Technological Research Council of Turkey (TÜBİTAK) in 2009.